

Insights into Laccase Engineering from Molecular Simulations: Toward a Binding-Focused Strategy

Emanuele Monza,[†] M. Fatima Lucas,[†] Susana Camarero,[‡] Lorea C. Alejandre,[‡] Angel T. Martínez,[‡] and Victor Guallar^{*,†,§}

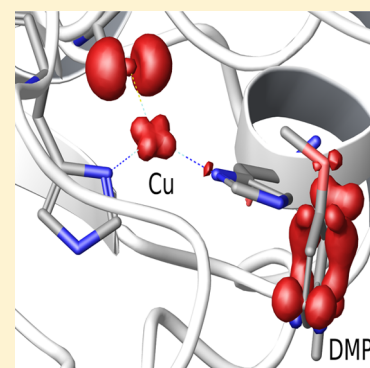
[†]Joint BSC-CRG-IRB Research Program in Computational Biology, Barcelona Supercomputing Center, c/Jordi Girona 29, 08034 Barcelona, Spain

[‡]Centro de Investigacion Biológica, CSIC, Ramiro de Maeztu 9, 28040 Madrid, Spain

[§]Institució Catalana de Recerca i Estudis Avançats (ICREA), Passeig Lluís Companys 23, 08010 Barcelona, Spain

Supporting Information

ABSTRACT: Understanding the molecular determinants of enzyme performance is of primary importance for the rational design of ad hoc mutants. A novel approach, which combines efficient conformational sampling and quick reactivity scoring, is used here to shed light on how substrate oxidation was improved during the directed evolution experiment of a fungal laccase (from *Pycnoporus cinnabarinus*), an industrially relevant class of oxidoreductases. It is found that the enhanced activity of the evolved enzyme is mainly the result of substrate arrangement in the active site, with no important change in the redox potential of the T1 copper. Mutations at the active site shift the binding mode into a more buried substrate position and provide a more favorable electrostatic environment for substrate oxidation. As a consequence, engineering the binding event seems to be a viable way to in silico evolution of oxidoreductases.



Enzyme engineering is a fast growing research field, mainly as a result of recent developments in directed evolution, rational mutagenesis, and in silico techniques.^{1,2} Laccases (EC 1.10.3.2) are multicopper oxidases that reduce oxygen to water through one-electron oxidation of a reducing substrate.^{3–5} Their broad substrate preference, the use of oxygen as final electron acceptor, and the production of water as sole byproduct make them suitable for sustainable chemistry.⁶ The active core of this class of enzymes consists of four copper ions arranged in two clusters: the T1 copper, placed in proximity of the protein surface, and the T2/T3 trinuclear cluster (TNC), buried in the protein interior. Four substrate molecules are oxidized in sequence by the T1 copper, which transfers the electrons, one by one, against an uphill redox potential gradient⁷ to the TNC, where oxygen is reduced. The overall correlation of the rate constant (k_{cat}) with the redox potential difference (ΔE°) between the T1 copper and the substrate^{8–10} suggests that (i) the T1 copper reduction is the rate-determining step of the catalytic process and (ii) the rate of this step is determined by the free energy difference between products and reactants. The latter point is likely a consequence of the high reorganization energy that accompanies substrate oxidation.^{10–12} For these reasons, the redox potential of the T1 copper, which ranges from 0.4 to 0.8 V versus normal hydrogen electrode (NHE), is considered to be the key parameter for substrate oxidation.³ Enhancing this quantity through mutagenesis would, in principle, allow us to speed up the oxidation of the existing substrates and expand the chemical space of

laccases. In this way, new doors to novel applications of these enzymes, which already encompass textile and food industry, bioremediation, forestry, and organic synthesis, would be opened.⁶

Even if some determinants of the redox potential of T1 are known,^{13–15} it is not clear yet how to effectively increase it. Furthermore, the ΔE° versus $\log k_{\text{cat}}$ correlation can show significant deviation from linearity.¹⁶ The oxidation of syringaldazine by *Rhizoctonia solani* (RsL) and *Myceliophthora thermophila* (MtL) laccases is a case in point.¹⁷ Although the redox potential of RsL is 250 mV higher than in MtL, its k_{cat} was found to be 8 times smaller.¹⁷ In another experiment, Xu and coworkers decreased the redox potential of *Trametes villosa* laccase (TvL) by 110 mV mutating the axial phenalanine to methionine: surprisingly, the turnover number slightly increased.¹⁸ Durão et al. showed that 93 and 60 mV increase in redox potential through mutation of the axial ligand in a bacterial laccase corresponded to a large decrease in k_{cat} against three different substrates.¹⁹ Apart from steric hindrance issues for bulky substrates,¹⁰ which can be overcome through site-directed mutagenesis of the enzyme pocket,²⁰ these deviations could be ascribed to the “goodness” of the Michaelis complex, meaning to which extent its structure serves or hinders the ET reaction. Indeed, its conformation has strong influence on: (i)

Received: February 2, 2015

Accepted: March 30, 2015

Table 1. Experimental Kinetic Data, Simulated Average Spin Density on Substrate (ρ_s substrate) and Copper with Its Coordinating Axial Atoms (ρ_s CuSNN), and Simulated Enzyme–Radical Stabilization of the Oxidation of DMP and ABTS by PcL (Wild Type) and 3PO (Mutant) at pH 5

system	K_M^a	k_{cat}^a	ρ_s substrate	ρ_s CuSNN	enzyme–radical stabilization ^b
PcL-ABTS	0.020 ± 0.001	35.1 ± 0.9	0.85	0.15	−89.4
PcL-DMP	0.012 ± 0.002	10.0 ± 0.3	0.37	0.63	−81.2
3PO-ABTS	0.024 ± 0.002	482.6 ± 10.2	0.96 (0.86, ^c 1.00 ^d)	0.04	−112.0
3PO-DMP	0.213 ± 0.013	196.9 ± 3.1	0.56 (0.34, ^e 0.66 ^f)	0.44	−110.8

^aExperimental data from ref 17. ^bValues in kcal/mol. ^cFigure 3C-like poses only (3). ^dFigure 3D-like poses only (4). ^eFigure 3A-like poses only (1). ^fFigure 3B-like poses only (2).

the electrostatic environment²¹ around the substrate which shifts its highest occupied molecular orbital (HOMO) energy perturbing its ionization potential²² and electronic coupling;¹² (ii) the solvent exposure of the complex, which affects reorganization energy;^{13,23} and (iii) the donor–acceptor distance, one of the main determinants of the electronic coupling.²⁴

In this work, we use a new simulation protocol to rationalize by first-principles the results of a recent²⁵ directed evolution study,² an experimental technique mimicking natural selection to evolve proteins toward a user-defined goal. We aim at a molecular understanding of how mutations accumulated through in vitro evolution lead to improved catalytic oxidation,²⁶ providing physicochemical grounds for future rational design efforts. In addition, we propose our protocol as an alternative for computational engineering of oxidoreductases. At the heart of our methodology is the combination of efficient conformational sampling techniques and quantum-chemical reactivity scoring based on changes in substrate's spin density. The enzyme–substrate conformational space nearby the T1 pocket is sampled with PELE,²⁷ a Monte Carlo algorithm that combines protein structure prediction algorithms with ligand and protein structural perturbations.²⁸ As recently shown, PELE quickly provides a complete protein–ligand energy landscape exploration (and free energies when combined with Markov state model analysis).²⁹ Then, 20 structures within 5 kcal/mol of the lowest binding energy pose are randomly selected and their reactivity scored evaluating the amount of spin density localized on the substrate with hybrid quantum mechanics–molecular mechanics (QM–MM) calculations.³⁰ Spin densities, which have been used to study oxidation mechanisms,^{31,32} estimate electron-transfer (ET) pathways^{33,34} and so on and show whether an unpaired electron is energetically more stable in donor or acceptor molecular orbitals. Therefore, its variations are expected to reflect changes in the ET driving force. This is confirmed in previous experimental studies, which reveal a linear relationship between the amount of spin density on the donor and its reduction/oxidation potential in ET proteins³⁵ and small aromatic compounds.³⁶ Moreover, preliminary calculations (details are provided in the Supporting Information (SI)) display a straight correlation between the spin density and the specificity constant of a number of para-substituted phenols (Table S1 and Figure S2 in the SI). Therefore, QM–MM spin densities are suitable to score ET reactivity. Along this descriptor, changes in electron coupling and solvent reorganization energy can be qualitatively predicted in terms of donor–acceptor distance^{24,37} and the substrate's solvent-accessible surface area (SASA)²³ of the poses generated with PELE. Monitoring these quantities is necessary: An increase in spin density upon mutation does not guarantee an improvement in

the rate constant if the donor–acceptor distance or SASA undergoes a large increase. Although a rigorous computation of Marcus equation's parameters is possible,^{38–41} this would be far more expensive and therefore unsuitable for screening a large number of mutants in a reasonable time, which is the ultimate goal of our PELE+QM–MM computational procedure.

The template laccase of our reference experiment is the *Pycnoporus cinnabarinus* laccase (PcL) and the substrates employed to screen activity are 2,2'-azino-bis(3-ethylbenzothiazoline-6-sulfonic acid) (ABTS) and 2,6-dimethoxyphenol (DMP).²⁵ As a result of the laboratory evolution, the turnover number significantly improved in the final mutant, 3PO, for both substrates (Table 1). The evolved laccase carries five mutations: P394H and N208S, which are located in the T1 pocket, N331D and D341N, relatively close to the substrate entrance, and R280H, located far away on the protein surface, mainly affecting protein expression in *Saccharomyces cerevisiae*²⁵ (Figure 1).

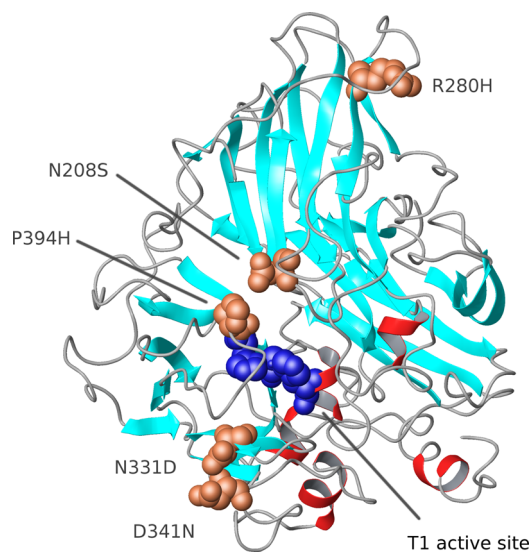


Figure 1. Structure of PcL where the active site T1 copper (and its coordination ligands) and mutated residues are highlighted in blue and light brown, respectively.

DMP Oxidation. In the first step of the simulation protocol, the enzyme–substrate system is sampled within 20 Å of the T1 copper with 240 independent PELE simulations, each lasting 48 h. According to the computational results, wild type and mutant have the same interaction energy with DMP, as shown in Figure 2A,B. The lowest energy bound structures reveal that PcL (wild type) has only one binding mode (1), also present in 3PO, depicted in red in Figure 2A,B. In this minimum DMP is hydrogen-bonded to H456 and D206 (Figure 3A), likely the

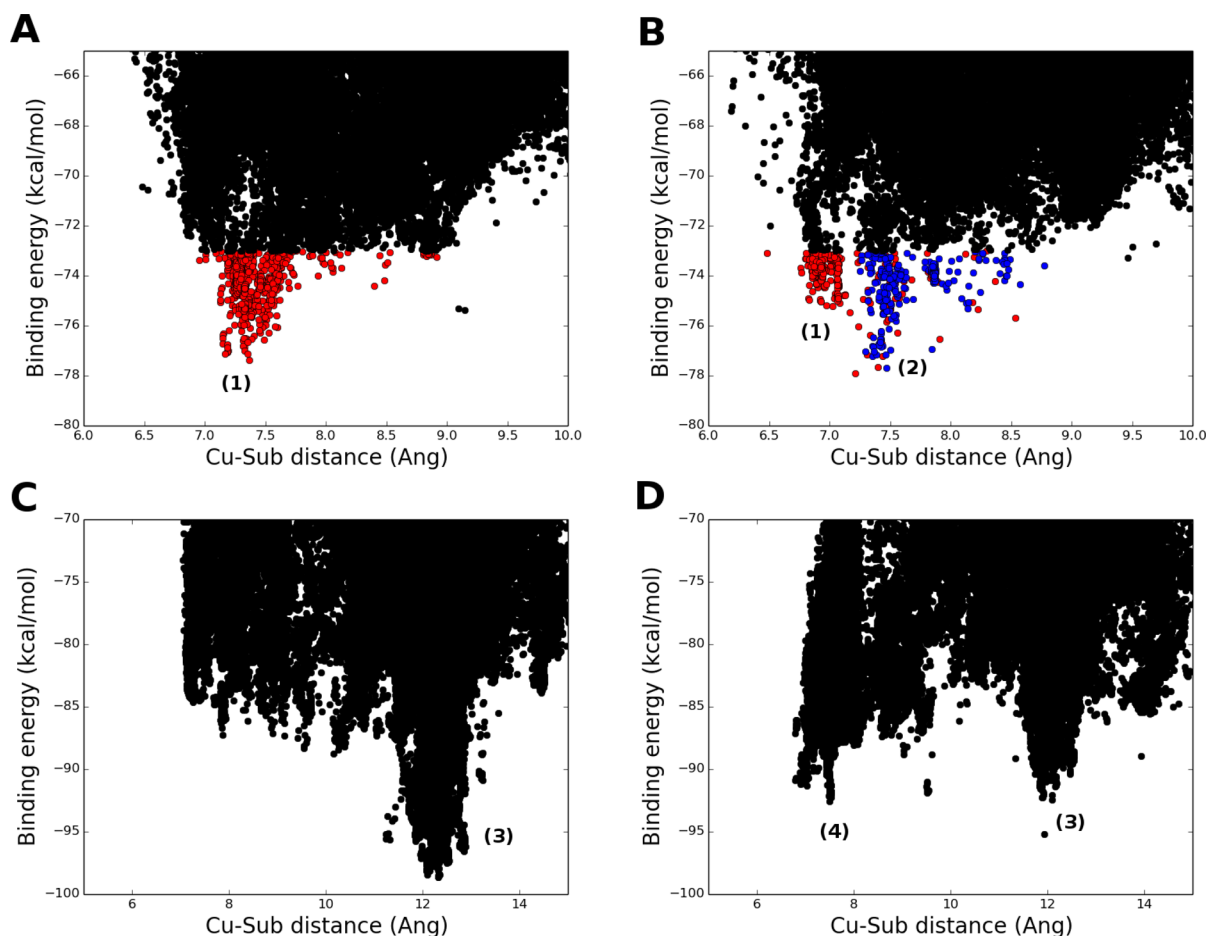


Figure 2. Results of PELE conformational search for DMP ((A) PcL, (B) 3PO) and ABTS ((C) PcL, (D) 3PO). “Cu-Sub distance” is the distance between the T1 copper and substrate’s center of mass. In panels A and B, binding modes similar to Figure 3A are represented in red, while binding modes similar to Figure 3B are in blue. Only structures within 5 kcal/mol of the best pose has been represented with colors. Numbers in parentheses label the binding modes depicted in Figure 3 and are used through the text.

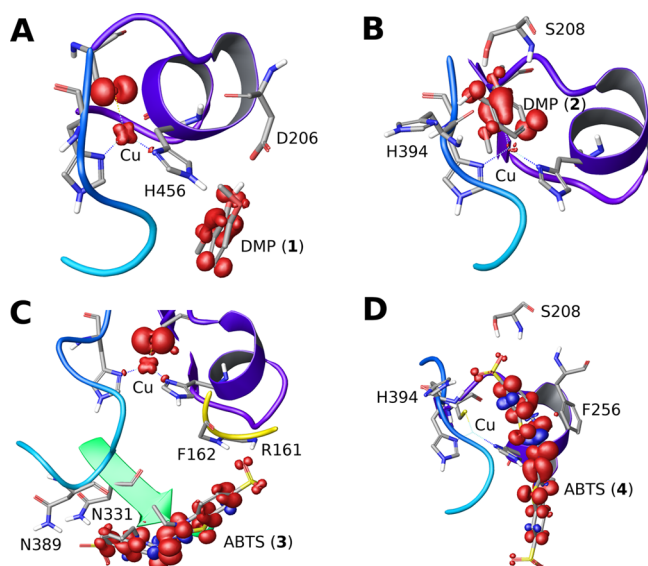


Figure 3. Most reactive binding modes of the enzyme–substrate complexes with spin density isosurfaces. Numbers in parentheses label each binding mode and are used through the text.

electron and proton acceptors, respectively.^{11,42} QM–MM scoring, applied to the 20 structures randomly selected within 5

kcal/mol of the lowest binding energy pose gives a result of 0.37 and 0.34 (Table 1) for PcL and 3PO, meaning that 37 and 34% of one electron charge flowed from DMP to the T1 copper center. Therefore, no improvement is found on passing from the wild type to the mutant for binding mode 1. P394H and N208S made room for an alternative enzyme–substrate conformation (2) in 3PO, represented in blue in Figure 2B, forming a hydrogen bond with H394 (Figure 3B). Importantly, the spin density of 2 is now 0.66 (Table 1), significantly higher than the one found for the wild type. Taking into account all of the 20 selected structures in 3PO (mixing 1 and 2, as shown in Figure 2B), the average substrate’s spin density is 0.56. The larger donor–acceptor distance in 2 with respect to 1 (Figure 2B) clearly indicates that focusing exclusively on this parameter is potentially misleading in ET rate scoring.

Structures within 3 Å RMSD of 2 represent only 0.2% of all of the conformations generated during PELE simulation in PcL, none of them within 5 kcal/mol of the lowest binding energy structure. On the contrary the occurrence of 2 is roughly 50% of the best 5 kcal/mol binding energy interval in 3PO. (Figure 2B). Then, oxidation is improved in the mutant by making this second and more reactive binding mode significantly available to the substrate. The increase in substrate’s spin density, which translates into a larger ET driving force, goes together with a reduction in donor–acceptor distance (Figure 2, for 1) and ligand’s SASA (Figure S6 in the SI), influencing electron

coupling and reorganization energy, resulting in an overall increase in k_{cat} .

Although K_{M} increased by almost the same amount as k_{cat} , most industrial applications of enzyme catalysts work at high substrate concentration. Under such conditions, k_{cat} is the most crucial component of catalytic efficiency. This is especially true for laccases, where substrate oxidation is the rate-determining step.¹⁰ For this reason, our aim is to efficiently score k_{cat} through the spin density rather than estimate K_{M} . Despite that, the K_{M} increase can be rationalized as well. As previously noted, protein–ligand interaction energies are virtually the same in PcL and 3PO (Figure 2A,B). Meanwhile k_{cat} largely improved, increasing the Michaelis constant (from steady-state approximation, $K_{\text{M}} = (k_{\text{off}} + k_{\text{cat}})/k_{\text{on}}$,⁴³ where k_{on} and k_{off} are the association and dissociation rate constants). Moreover, having two highly accessible reacting binding modes that can be filled simultaneously (as shown with ligand docking using Glide,^{44,45} Figure S4 in the SI) requires a higher concentration of substrate to reach half of the maximum reaction rate.⁴³

ABTS Oxidation. When simulating ABTS binding with PELE (240 independent trajectories, 48 h each), a sharp minimum (3) is located next to the active site in the wild-type Laccase (Figure 3C). In the corresponding structures, ABTS forms multiple hydrogen bonds; one of ABTS negatively charged sulfonate groups interacts with N331 and N389, while the other one interacts with two backbone hydrogens (Figure 3C). QM–MM calculations yield an average substrate's spin density of 0.85 for 3. Because of the N331D mutation, one stabilizing asparagine–sulfonate interaction no longer occurs in 3PO, and the depth of the previously mentioned minimum is sensibly reduced (Figure 2D). Simultaneously the enzyme–substrate interaction inside the T1 pocket is stabilized, as can be seen by the clear appearance of a second minimum (4) within 8 Å of the T1 copper. As a consequence, approximately one half of the 20 randomly picked structures populate this second minimum, interacting with S208 and H394 (Figure 3D). The overall substrate's spin density for 3PO is 0.96 (being 1.00 for 4 and 0.86 for 3). It is important to bear in mind that absolute values have limited physical meaning and attention should be paid only to relative values within the same substrate. Similarly to DMP, the most reactive pose, 4, is poorly accessible to the native enzyme (5% occurrence) and never observed within 5 kcal/mol of the lowest binding energy value (Figure 2C). Therefore, ABTS oxidation is improved by refining substrate recognition, shifting the population in favor of the most reactive binding mode, as observed for DMP oxidation. Moreover, in ABTS the average decrease in donor–acceptor distance and solvent exposure is more accentuated. (The substrate docks deeper inside the protein.)

The experimental K_{M} did not change significantly for ABTS. This can be justified as a compensation between increased affinity at 4 and higher rate constant because $K_{\text{M}} = (k_{\text{off}} + k_{\text{cat}})/k_{\text{on}}$. Moreover, contrary to DMP, at substrate saturation the coexistence of 3 and 4 is implausible because ABTS carries two negative charges that would repel each other at such a close distance.

Redox Potential. To evaluate the possible effects of directed evolution on T1 copper redox potential, we carried out two sets of 5 ns molecular dynamics (MD) simulations of PcL and 3PO (with no substrate), both in their oxidized and reduced states, for a total of 8 (2 × 4) trajectories. Then, 10 equally spaced snapshots in the 3.2 to 5.0 ns time interval were extracted from each trajectory, and the $\Delta\Delta G$ of T1 copper reduction was

estimated with the linear response approximation^{15,39} (LRA). The calculated $\Delta\Delta G$ is -0.84 and 0.70 kcal/mol in the first and second set of MD simulations, respectively (+36 and -31 mV), well below the accuracy of the method. Therefore, according to the MD simulations, the redox potential is substantially unchanged after laboratory evolution (as expected, only P394H involves T1 copper's second coordination sphere). The driving force determinant must then originate from radical substrate (oxidized product) stabilization or reactant destabilization, the latter being discarded because enzyme–substrate interaction energies are unchanged in DMP and even improved, in the T1 pocket, in the case of ABTS (Figure 2).

Determinants of the Driving Force Improvement. As previously stated, the reaction rate is mostly driven by the free-energy difference between product and reactant of the first oxidation step.¹⁰ This driving force is equal to the redox potential difference between T1 copper and the oxidized substrate. Because the metal redox potential and protein–reactant interaction energies remain nearly identical in the mutant, optimization of the enzyme pocket toward the oxidized substrate must play a major role. To assess this point, we set up a new PELE simulation (48 independent trajectories, 48 h each) in which the substrate is modeled in its oxidized state. This is done using the atomic charges obtained from the quantum geometry optimization of the oxidized (radical) species. (Details of substrate parametrization are provided in the SI.) In such a way, the enzyme–substrate interaction energy represents the degree of stabilization of the oxidized substrate by the protein environment. As shown in the last column of Table 1, 3PO turned out to be clearly a more favorable host for the oxidized species than PcL because the minimum substrate–enzyme classical (force field) interaction energy is significantly lower in the mutant (Table 1). Notably, these classical simulations results (improved enzyme–radical stabilization in 3PO, Table 1) agree with the increase in substrate's spin density seen in the (slow/expensive) quantum-mechanics simulations. Such scenario opens the door to implement fast computational screening of mutants using PELE's ligand sampling, which requires ~ 10 h × 8 CPUs per mutant, to improve the enzyme–radical interaction energy through several mutation cycles. Subsequent spin density calculations can be used at the end of each cycle to rescore the most promising mutants.

In conclusion, molecular simulations indicate that mutations accumulated during directed evolution increase laccases enzymatic activity by affecting substrate binding rather than the metal redox potential. Extensive conformational sampling revealed important changes in the protein–ligand energy landscape upon mutation. Then, quantum-chemical calculations confirmed an oxidation (substrate's spin density) increase as a result of an enhanced electrostatic stabilization of the radical species. No significant change is detected in the T1 copper redox potential. Therefore, the oxidation rate of a target substrate can be improved by fine-tuning the binding event. In the authors' opinion, this is a viable way to the design of fit-for-purpose laccases (extendable to other oxidative enzymes), which might be undertaken with the assistance of computational methodologies like the one presented here.

METHODS

System Setup. The PcL structure (2XYB) is taken from the Protein Data Bank and prepared with Protein Preparation Wizard⁴⁶ at pH 5 to compare with the experimental data. The

protonation state of titratable residues is generated with PROPKA⁴⁷ and double-checked by visual inspection and comparison with the outcome of the H++ server (<http://biophysics.cs.vt.edu/H++>).⁴⁸ Four acidic residues are, according to both methods, protonated: 50, 440, 454, and 468. 3PO mutations are introduced, and the new protein structure is relaxed with PELE.

PELE Sampling. PELE is a Monte Carlo algorithm in which a move consists of three steps: perturbation, relaxation, and Metropolis acceptance criteria. First, the ligand is subjected to random rotations and translations while the protein is perturbed based on the anisotropic network model (ANM);⁴⁹ all of the atoms are displaced by a minimization where the α -carbons are forced to follow a linear combination of randomly picked low eigenvector obtained in the ANM approach. This perturbation stage is followed by discrete minimization⁵⁰ of those side chains with higher energy increase along the previous ANM step. Finally, a truncated Newton minimization, using the OPLS⁵¹ all-atom force field and an implicit surface-generalized Born continuum solvent,⁵² is performed to obtain a new local structure. Along the text, PELE's binding energy refers to protein–substrate interaction potential energies. After PELE's sampling, 20 structures within 5 kcal/mol of the lowest binding energy pose are randomly selected for QM-MM analysis.

QM-MM Reactivity Scoring. Structures are relaxed with five steps of geometry optimization using Qsite,⁵³ and the spin density of the substrate is evaluated using Mulliken partitioning method.⁵⁴ Substrate, T1 copper, and its first coordination sphere are included in the quantum region, while the rest of the protein is treated classically. The density functional method with the M06⁵⁵ functional and the lacvp^{*56,57} basis set is used for the quantum region, while the OPLS-AA⁵¹ force field is used for the classical part. A nonbonded cutoff of 50 Å is applied. The partial geometry optimization is found to be sufficient to let the spin density virtually converge, as clearly visible in Figure S3 in the SI. Solvent effects are neglected to speed up the calculations (saving both CPU time of a single geometry optimization and sensibly reducing the number of calculations because the effect of water MM charges would need to be averaged on a much larger number of structures). Although this choice leads to errors on an absolute ground, the error is most likely comparable for all of the poses involving the same ligand, making relative estimation still reliable (while absolute values are not expected to be meaningful). Indeed, the final aim of this methodology is to screen the activity of a big number of mutants toward the same substrate. Solvent effects can potentially be extrapolated and discussed, inspecting changes in substrate's SASA.²³

Molecular Dynamics. System preparation (creation of orthorhombic box with a minimum distance of 10 Å between the protein surface and box's wall, solvation with explicit waters, neutralization, and addition of 0.15 M NaCl), equilibration (Desmond's default protocol), and the 5 ns NPT production phase at 300 K are performed with Desmond.⁵⁸ The OPLS-2005 force field⁵¹ and the SPC explicit water model is used. The temperature is regulated with the Nosé–Hoover chain thermostat⁵⁹ with a relaxation time of 1.0 ps, and the pressure is controlled with the Martyna–Tobias–Klein barostat⁶⁰ with isotropic coupling and a relaxation time of 2.0 ps. The RESPA integrator⁶¹ is employed with bonded, near, and far time steps of 2.0, 2.0, and 6.0 fs, respectively. A 9 Å cutoff is used for nonbonded interactions together with the smooth particle mesh Ewald method.⁶²

$\Delta\Delta G$ Calculation. The structures selected from each MD trajectory are treated at the same level of theory used for the reactivity scoring (see QM–MM Reactivity Scoring), with the only difference being that an 8 Å layer of explicit water molecules around the protein is kept and geometry optimization is now complete. Although more waters would be necessary to accurately estimate the absolute ΔG (to guarantee an appropriate electrostatic description of the system), the systematic error introduced here is the same for wild-type and mutant protein. After QM–MM minimization, an electron is added (removed) from the reduced (oxidized) relaxed state and a single point calculation is performed at the same level of theory. Vertical energies are calculated as the difference between single point and geometry optimized energies. Then, $\Delta\Delta G$ of reduction is estimated using the LRA^{15,39} as

$$\Delta\Delta G = 1/2[(\Delta V_{\text{CU(III)}} - \Delta V_{\text{CU(I)}})_{3\text{PO}} - (\Delta V_{\text{CU(III)}} - \Delta V_{\text{CU(I)}})_{\text{PELE}}]$$

where ΔV_i is the vertical energy of the oxidation state i .

■ ASSOCIATED CONTENT

📄 Supporting Information

Validation of the spin density as a suitable quantum-chemical descriptor, ligand's template generation with PELE, docking of two molecules of DMP in 3PO's active site, PELE's binding energy plots for the radical species, ligand's SASA versus distance plots, heavy atom RMSD of MD simulations. This material is available free of charge via the Internet at <http://pubs.acs.org>.

■ AUTHOR INFORMATION

Corresponding Author

*E-mail: victor.guallar@bsc.es.

Notes

The authors declare no competing financial interest.

■ ACKNOWLEDGMENTS

This work has been funded by the EU projects INDOX (KBBE-2013-7-613549) and ERC 2009-Adg25027-PELE (to V.G) and the Spanish Ministry of Education and Science project CTQ2013-48287 (to V.G).

■ REFERENCES

- (1) Nanda, V.; Koder, R. L. Designing Artificial Enzymes by Intuition and Computation. *Nat. Chem.* **2010**, *2*, 15–24.
- (2) Tracewell, C. A.; Arnold, F. H. Directed Enzyme Evolution: Climbing Fitness Peaks One Amino Acid at a Time. *Curr. Opin. Chem. Biol.* **2009**, *13*, 3–9.
- (3) Giardina, P.; Faraco, V.; Pezzella, C.; Piscitelli, A.; Vanhulle, S.; Sannia, G. Laccases: A Never-Ending Story. *Cell. Mol. Life Sci.* **2010**, *67*, 369–385.
- (4) Morozova, O. V.; Shumakovich, G. P.; Gorbacheva, M. A.; Shleev, S. V.; Yaropolov, A. I. Blue[™] Laccases. *Biochemistry (Moscow)* **2007**, *72*, 1136–1150.
- (5) Solomon, E. I.; Sundaram, U. M.; Machonkin, T. E. Multicopper Oxidases and Oxygenases. *Chem. Rev.* **1996**, *96*, 2563–2606.
- (6) Riva, S. Laccases: Blue Enzymes for Green Chemistry. *Trends Biotechnol.* **2006**, *24*, 219–226.
- (7) Ramírez, P.; Mano, N.; Andreu, R.; Ruzgas, T.; Heller, A.; Gorton, L.; Shleev, S. Direct Electron Transfer from Graphite and Functionalized Gold Electrodes to T1 and T2/T3 Copper Centers of

- Bilirubin Oxidase. *Biochim. Biophys. Acta, Bioenerg.* **2008**, *1777*, 1364–1369.
- (8) Xu, F. Oxidation of Phenols, Anilines, and Benzenethiols by Fungal Laccases: Correlation between Activity and Redox Potentials as Well as Halide Inhibition†. *Biochemistry (Moscow)* **1996**, *35*, 7608–7614.
- (9) Xu, F.; Kulys, J. J.; Duke, K.; Li, K.; Krikstopaitis, K.; Deussen, H.-J. W.; Abbate, E.; Galinyte, V.; Schneider, P. Redox Chemistry in Laccase-Catalyzed Oxidation of N-Hydroxy Compounds. *Appl. Environ. Microbiol.* **2000**, *66*, 2052–2056.
- (10) Tadesse, M. A.; D'Annibale, A.; Galli, C.; Gentili, P.; Sergi, F. An Assessment of the Relative Contributions of Redox and Steric Issues to Laccase Specificity towards Putative Substrates. *Org. Biomol. Chem.* **2008**, *6*, 868–878.
- (11) Galli, C.; Madzak, C.; Vadalà, R.; Jolival, C.; Gentili, P. Concerted Electron/Proton Transfer Mechanism in the Oxidation of Phenols by Laccase. *ChemBioChem.* **2013**, *14*, 2500–2505.
- (12) Marcus, R. A. Electron Transfer Reactions in Chemistry. Theory and Experiment. *Rev. Mod. Phys.* **1993**, *65*, 599–610.
- (13) Hong, G.; Ivnitski, D. M.; Johnson, G. R.; Atanassov, P.; Pachter, R. Design Parameters for Tuning the Type 1 Cu Multicopper Oxidase Redox Potential: Insight from a Combination of First Principles and Empirical Molecular Dynamics Simulations. *J. Am. Chem. Soc.* **2011**, *133*, 4802–4809.
- (14) Li, H.; Webb, S. P.; Ivanic, J.; Jensen, J. H. Determinants of the Relative Reduction Potentials of Type-1 Copper Sites in Proteins. *J. Am. Chem. Soc.* **2004**, *126*, 8010–8019.
- (15) Olsson, M. H. M.; Hong, G.; Warshel, A. Frozen Density Functional Free Energy Simulations of Redox Proteins: Computational Studies of the Reduction Potential of Plastocyanin and Rusticyanin. *J. Am. Chem. Soc.* **2003**, *125*, 5025–5039.
- (16) Xu, F.; Shin, W.; Brown, S. H.; Wahleithner, J. A.; Sundaram, U. M.; Solomon, E. I. A Study of a Series of Recombinant Fungal Laccases and Bilirubin Oxidase That Exhibit Significant Differences in Redox Potential, Substrate Specificity, and Stability. *Biochim. Biophys. Acta, Protein Struct. Mol. Enzymol.* **1996**, *1292*, 303–311.
- (17) Xu, F.; Berka, R. M.; Wahleithner, J. A.; Nelson, B. A.; Shuster, J. R.; Brown, S. H.; Palmer, A. E.; Solomon, E. I. Site-Directed Mutations in Fungal Laccase: Effect on Redox Potential, Activity and pH Profile. *Biochem. J.* **1998**, *334*, 63–70.
- (18) Xu, F.; Palmer, A. E.; Yaver, D. S.; Berka, R. M.; Gambetta, G. A.; Brown, S. H.; Solomon, E. I. Targeted Mutations in a *Trametes villosa* Laccase Axial Perturbations of The T1 Copper. *J. Biol. Chem.* **1999**, *274*, 12372–12375.
- (19) Durão, P.; Bento, I.; Fernandes, A. T.; Melo, E. P.; Lindley, P. F.; Martins, L. O. Perturbations of the T1 Copper Site in the CotA Laccase from *Bacillus subtilis*: Structural, Biochemical, Enzymatic and Stability Studies. *JBIC, J. Biol. Inorg. Chem.* **2006**, *11*, 514–526.
- (20) Galli, C.; Gentili, P.; Jolival, C.; Madzak, C.; Vadalà, R. How Is the Reactivity of Laccase Affected by Single-Point Mutations? Engineering Laccase for Improved Activity towards Sterically Demanding Substrates. *Appl. Microbiol. Biotechnol.* **2011**, *91*, 123–131.
- (21) Warshel, A.; Sharma, P. K.; Kato, M.; Xiang, Y.; Liu, H.; Olsson, M. H. M. Electrostatic Basis for Enzyme Catalysis. *Chem. Rev.* **2006**, *106*, 3210–3235.
- (22) Koopmans, T. Über Die Zuordnung von Wellenfunktionen Und Eigenwerten Zu Den Einzelnen Elektronen Eines Atoms. *Physica* **1934**, *1*, 104–113.
- (23) Bortolotti, C. A.; Siwko, M. E.; Castellini, E.; Ranieri, A.; Sola, M.; Corni, S. The Reorganization Energy in Cytochrome c Is Controlled by the Accessibility of the Heme to the Solvent. *J. Phys. Chem. Lett.* **2011**, *2*, 1761–1765.
- (24) Winkler, J. R.; Gray, H. B. Electron Flow through Metalloproteins. *Chem. Rev.* **2013**, *114* (7), 3369–3380.
- (25) Camarero, S.; Pardo, I.; Canas, A. I.; Molina, P.; Record, E.; Martinez, A. T.; Martinez, M. J. Alcalde, M. Engineering Platforms for Directed Evolution of Laccase from *Pycnoporus cinnabarinus*. *Appl. Environ. Microbiol.* **2012**, *78*, 1370–1384.
- (26) Pardo, I.; Camarero, S. Laccase Engineering by Rational and Evolutionary Design. *Cell. Mol. Life Sci.* **2015**, 1–14.
- (27) Borrelli, K. W.; Vitalis, A.; Alcantara, R.; Guallar, V. PELE: Protein Energy Landscape Exploration. A Novel Monte Carlo Based Technique. *J. Chem. Theory Comput.* **2005**, *1*, 1304–1311.
- (28) Cossins, B. P.; Hosseini, A.; Guallar, V. Exploration of Protein Conformational Change with PELE and Meta-Dynamics. *J. Chem. Theory Comput.* **2012**, *8*, 959–965.
- (29) Takahashi, R.; Gil, V. A.; Guallar, V. Monte Carlo Free Ligand Diffusion with Markov State Model Analysis and Absolute Binding Free Energy Calculations. *J. Chem. Theory Comput.* **2014**, *10*, 282–288.
- (30) Senn, H. M.; Thiel, W. QM/MM Methods for Biomolecular Systems. *Angew. Chem., Int. Ed.* **2009**, *48*, 1198–1229.
- (31) Johansson, M. P.; Blomberg, M. R. A.; Sundholm, D.; Wikström, M. Change in Electron and Spin Density upon Electron Transfer to Haem. *Biochim. Biophys. Acta, Bioenerg.* **2002**, *1553*, 183–187.
- (32) Catlow, C. R. A.; French, S. A.; Sokol, A. A.; Thomas, J. M. Computational Approaches to the Determination of Active Site Structures and Reaction Mechanisms in Heterogeneous Catalysts. *Philos. Trans. R. Soc., A* **2005**, *363*, 913–936.
- (33) Guallar, V.; Wallrapp, F. Mapping Protein Electron Transfer Pathways with QM/MM Methods. *J. R. Soc. Interface* **2008**, *5*, S233–S239.
- (34) Guallar, V. Heme Electron Transfer in Peroxidases: The Propionate E-Pathway. *J. Phys. Chem. B* **2008**, *112*, 13460–13464.
- (35) Artz, K.; Williams, J. C.; Allen, J. P.; Lendzian, F.; Rautter, J.; Lubitz, W. Relationship between the Oxidation Potential and Electron Spin Density of the Primary Electron Donor in Reaction Centers from *Rhodobacter sphaeroides*. *Proc. Natl. Acad. Sci. U. S. A.* **1997**, *94*, 13582–13587.
- (36) Meisel, D.; Neta, P. One-Electron Redox Potentials of Nitro Compounds and Radiosensitizers. Correlation with Spin Densities of Their Radical Anions. *J. Am. Chem. Soc.* **1975**, *97*, 5198–5203.
- (37) Christensen, N. J.; Kepp, K. P. Setting the Stage for Electron Transfer: Molecular Basis of ABTS-Binding to Four Laccases from *Trametes versicolor* at Variable pH and Protein Oxidation State. *J. Mol. Catal. B: Enzym.* **2014**, *100*, 68–77.
- (38) Wallrapp, F. H.; Voityuk, A. A.; Guallar, V. In-Silico Assessment of Protein-Protein Electron Transfer. A Case Study: Cytochrome c Peroxidase – Cytochrome c. *PLoS Comput. Biol.* **2013**, *9*, e1002990.
- (39) Blumberger, J. Free Energies for Biological Electron Transfer from QM/MM Calculation: Method, Application and Critical Assessment. *Phys. Chem. Chem. Phys.* **2008**, *10*, 5651–5667.
- (40) Hu, L.; Farrokhnia, M.; Heimdal, J.; Shleev, S.; Rulišek, L.; Ryde, U. Reorganization Energy for Internal Electron Transfer in Multicopper Oxidases. *J. Phys. Chem. B* **2011**, *115*, 13111–13126.
- (41) Voityuk, A. A.; Rösch, N. Fragment Charge Difference Method for Estimating Donor–acceptor Electronic Coupling: Application to DNA Π -Stacks. *J. Chem. Phys.* **2002**, *117*, 5607–5616.
- (42) Matera, I.; Gullotto, A.; Tilli, S.; Ferraroni, M.; Scozzafava, A.; Briganti, F. Crystal Structure of the Blue Multicopper Oxidase from the White-Rot Fungus *Trametes trogii* Complexed with P-Toluolate. *Inorg. Chim. Acta* **2008**, *361*, 4129–4137.
- (43) Lehninger, A. L.; Nelson, D. L.; Cox, M. M. *Lehninger Principles of Biochemistry*; W. H. Freeman: New York, 2005.
- (44) Friesner, R. A.; Banks, J. L.; Murphy, R. B.; Halgren, T. A.; Klicic, J. J.; Mainz, D. T.; Repasky, M. P.; Knoll, E. H.; Shelley, M.; Perry, J. K.; et al. Glide: A New Approach for Rapid, Accurate Docking and Scoring. 1. Method and Assessment of Docking Accuracy. *J. Med. Chem.* **2004**, *47*, 1739–1749.
- (45) Halgren, T. A.; Murphy, R. B.; Friesner, R. A.; Beard, H. S.; Frye, L. L.; Pollard, W. T.; Banks, J. L. Glide: A New Approach for Rapid, Accurate Docking and Scoring. 2. Enrichment Factors in Database Screening. *J. Med. Chem.* **2004**, *47*, 1750–1759.
- (46) Sastry, G. M.; Adzhigirey, M.; Day, T.; Annabhimoju, R.; Sherman, W. Protein and Ligand Preparation: Parameters, Protocols, and Influence on Virtual Screening Enrichments. *J. Comput.-Aided Mol. Des.* **2013**, *27*, 221–234.

(47) Olsson, M. H. M.; Søndergaard, C. R.; Rostkowski, M.; Jensen, J. H. PROPKA3: Consistent Treatment of Internal and Surface Residues in Empirical pKa Predictions. *J. Chem. Theory Comput.* **2011**, *7*, 525–537.

(48) Anandkrishnan, R.; Aguilar, B.; Onufriev, A. V. H++ 3.0: Automating pK Prediction and the Preparation of Biomolecular Structures for Atomistic Molecular Modeling and Simulations. *Nucleic Acids Res.* **2012**, *40*, W537–W541.

(49) Atilgan, A. R.; Durell, S. R.; Jernigan, R. L.; Demirel, M. C.; Keskin, O.; Bahar, I. Anisotropy of Fluctuation Dynamics of Proteins with an Elastic Network Model. *Biophys. J.* **2001**, *80*, 505–515.

(50) Jacobson, M. P.; Kaminski, G. A.; Friesner, R. A.; Rapp, C. S. Force Field Validation Using Protein Side Chain Prediction. *J. Phys. Chem. B* **2002**, *106*, 11673–11680.

(51) Kaminski, G. A.; Friesner, R. A.; Tirado-Rives, J.; Jorgensen, W. L. Evaluation and Reparametrization of the OPLS-AA Force Field for Proteins via Comparison with Accurate Quantum Chemical Calculations on Peptides. *J. Phys. Chem. B* **2001**, *105*, 6474–6487.

(52) Bashford, D.; Case, D. A. Generalized Born Models of Macromolecular Solvation Effects. *Annu. Rev. Phys. Chem.* **2000**, *51*, 129–152.

(53) Murphy, R. B.; Philipp, D. M.; Friesner, R. A. A Mixed Quantum Mechanics/molecular Mechanics (QM/MM) Method for Large-Scale Modeling of Chemistry in Protein Environments. *J. Comput. Chem.* **2000**, *21*, 1442–1457.

(54) Mulliken, R. S. Electronic Population Analysis on LCAO–MO Molecular Wave Functions. I. *J. Chem. Phys.* **1955**, *23*, 1833–1840.

(55) Zhao, Y.; Truhlar, D. G. The M06 Suite of Density Functionals for Main Group Thermochemistry, Thermochemical Kinetics, Non-covalent Interactions, Excited States, and Transition Elements: Two New Functionals and Systematic Testing of Four M06-Class Functionals and 12 Other Functionals. *Theor. Chem. Acc.* **2008**, *120*, 215–241.

(56) Hay, P. J.; Wadt, W. R. Ab Initio Effective Core Potentials for Molecular Calculations. Potentials for the Transition Metal Atoms Sc to Hg. *J. Chem. Phys.* **1985**, *82*, 270–283.

(57) Hehre, W. J.; Ditchfield, R.; Pople, J. A. Self-Consistent Molecular Orbital Methods. XII. Further Extensions of Gaussian-Type Basis Sets for Use in Molecular Orbital Studies of Organic Molecules. *J. Chem. Phys.* **1972**, *56*, 2257–2261.

(58) *Desmond Molecular Dynamics System*, version 3.1; D. E. Shaw Research: New York, 2012.

(59) Nosé, S. A Unified Formulation of the Constant Temperature Molecular Dynamics Methods. *J. Chem. Phys.* **1984**, *81*, 511–519.

(60) Martyna, G. J.; Tobias, D. J.; Klein, M. L. Constant Pressure Molecular Dynamics Algorithms. *J. Chem. Phys.* **1994**, *101*, 4177–4189.

(61) Tuckerman, M.; Berne, B. J.; Martyna, G. J. Reversible Multiple Time Scale Molecular Dynamics. *J. Chem. Phys.* **1992**, *97*, 1990–2001.

(62) Essmann, U.; Perera, L.; Berkowitz, M. L.; Darden, T.; Lee, H.; Pedersen, L. G. A Smooth Particle Mesh Ewald Method. *J. Chem. Phys.* **1995**, *103*, 8577–8593.